Effect of an Imidazoline Derivative on the Protection Performance of Oxide Film Formed on Carbon Steel in Saturated Ca(OH)$_2$ Solution

Lijuan Feng, Huaiyu Yang[*]*, Fuhui Wang*

State Key Laboratory for Corrosion and Protection, Institute of Metal Research, Chinese Academy of Sciences, Shenyang 110016, China
[*]E-mail: hyyang@imr.ac.cn

The effect of a stearic imidazoline derivative, namely, 1-[N,N'-bis(hydroxylethylether) –aminoethyl]-2-stearicimidazoline (HASI) on the protective property of oxide film formed on the carbon steel in saturated Ca(OH)$_2$ solution was investigated by electrochemical measurements in conjunction with Raman spectroscopy technique. Computational simulations and point defect model (PDM) were also employed to elucidate the influence of inhibitor on the oxide film formed on carbon steel surface. The results indicated that HASI can effectively retard the carbon steel corrosion in alkaline solution by suppressing dominantly the cathodic reduction of oxygen. The addition of the inhibitor can enhance the stability of Fe$_3$O$_4$ to be further oxidized into ferric species and lead to the formation of a more compact protective film on carbon steel surface, and then reduces the defect density in the surface film and improve its protective property.

1. INTRODUCTION

Since the invention of Portland cement, reinforced concrete structures have been widely used in various construction fields. Generally, steel rebar in the concrete is under a passive state due to an oxide film is formed on its surface, which significantly suppresses its corrosion. However, as time goes by, the concrete structure gradually deteriorates because of the corrosion of steel rebar [1-5]. It has been reported that the reinforment corrosion is one of the major causes of degradation of concrete structures [6]. Thus, the most effective solution to mitigate the degradation of concrete structes is to inhibit the steel rebar corrosion. There are mainly two factors that cause the steel rebar corrosion. The one is kown as the carbonization of the concrete, namely, CO$_2$ in the atmosphere reacts with the

alkaline substances in concrete, leading to the decrease of pH value and consequently causing the dissolution of the passive film. The other one is that aggressive ions (such as Cl^-) in their service enviroment penetrate through the concrete structures and reach the steel surface, resulting in the local depassivation of the steel rebar and inducing pitting corrosion [7-9]. Obviously, the properties of the oxide film play a siganificant role in the steel rebar corrosion. Therefore, one of the most important solutions to mitigate the steel rebar corrosion is to improve the corrosion resistance of oxide layer and this can be well achieved by applying the corrosion inhibitors in its service enviroment [1,9-11].

Due to there are multiple functional groups in the molecular structure, imidazoline derivatives favor to adsorb on the metal surface and form an protective film so that they are often used as effective corrosion inhibitors of zinc and copper in akaline solution [12,13]. Quite recently, our research also demonstrated that a stearic imidazoline derivative can effectively inhibit the corrosion of carbon steel in alkaline chloride solution [14]. Up to our knowledge, however, the effect of such an inhibitor on the properties of oxide film formed on the carbon steel surface in alkaline solution is still not clear. Therefore, in the present paper, the influence of a imidazoline derivative (HASI) on the charateristics of oxide film formed on carbon steel surface in the saturated $Ca(OH)_2$ solution was investigated by electrochemical measurements and Raman spectroscopy technique, as well as computational modeling. The point defects model (PDM) was employed to elucidate the inhibition mechanism of the inhibitor.

2. EXPERIMENT

2.1. Samples and test solution preparation

The test medium used in all experiments was a saturated $Ca(OH)_2$ solution (pH 12.5), which was prepared by the reagent grade $Ca(OH)_2$ and bi-distill water. The inhibitor tested was a type of stearic imidazoline derivatives, which was purchased from Yixing Chemical Co. as high grade reagent and used without further purification. All the measurements were carried out under open to air conditions and at room temperature.

The working electrodes used for all electrochemical measurements were cut from the steel rebar (0.15% C; 0.15% Si; 0.44% Mn; 0.30% P; 0.03% S and balance Fe) and then embedded in an epoxy resin leaving an exposed working area of 0.50 cm^2. Before each experiment, the working electrode was ground gradually with emery paper up to 800 grade, then washed with distilled water, degreased in acetone and dried with cool air.

2.2. Electrochemical measurements

Electrochemical experiments were performed with PARSTAT 2273 electrochemical system (Princeton Applied Research) equipped with a conventional three electrodes cell. A large platinum plate of 2.0 cm × 2.0 cm was used as the counter electrode and a saturated calomel electrode (SCE) with a Luggin capillary as the reference electrode. Prior to each experiment, the working electrode was immersed in the test solution with and without the addition of an inhibitor for 3 days at the open circuit

potential (OCP) to reach a steady potential. The potentiodynamic polarization was started from −250 mV versus OCP to the potential at which the current density increased abruptly with a scan rate of 1 mV s^{-1}. The electrochemical impedance spectroscopy (EIS) was carried out in the frequency range of 100 kHz to 10 mHz with an amplitude of 10 mV peak-to-peak, using AC signals at the OCP. The cyclic voltammetry and Mott–Schottky curves were recorded from −1.2 V to 0.8 V (SCE) with a scan rate of 20 mV s^{-1} after 30 min immersion in the test solution.

2.3 Raman spectrum analysis

The samples used for Raman spectrum analysis were prepared from the same steel rebar used in the electrochemical tests. Before each experiment, the carbon steel sample was roughened down to 2.5 µm and then immersed in the test solutions with and without the inhibitor for 3 days. After the specimen was brought out, the surface was analyzed by a confocal microprobe Raman system (JY HB800) with the excitation laser line of 632.8 nm at the range of 200 cm^{-1} to 800 cm^{-1}.

2.4 Computational modeling

Computational modeling was conducted using the Discover module of the Materials Studio 5.0 package (Accelrys Co.). The computational model unit was constructed with three layers. The bottom layer was a constraint Fe(1 1 1) surface, and the middle one was built by cleaving a Fe_3O_4(1 1 1) surface which was not frozen during the process of simulation. The top layer was solution layer, which was unconstraint and contained 100 water molecules with and without 3 HASI molecules, respectively. These models were optimized by the Smart Minimizer method until the system had the lowest energy.

3. RESULTS AND DISCUSSION

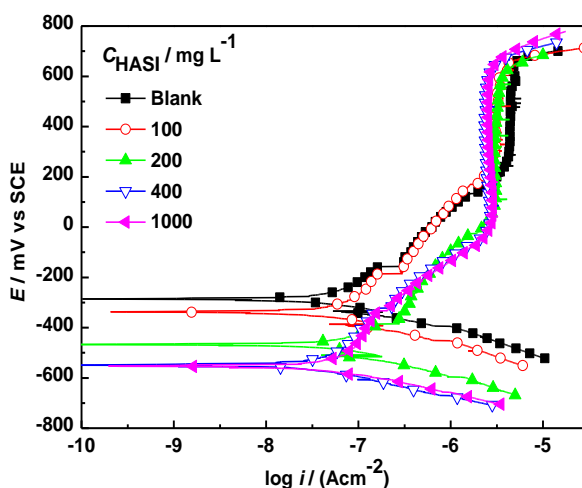### 3.1 Potentiodynamic polarization and cyclic voltammetry measurements

Figure 1. Polarization curves of carbon steel samples in saturated Ca(OH)$_2$ solutions with different concentrations of HASI

Table 1. The electrochemical parameters obtained from the polarization data

Conc. mg L^{-1}	Ecorr mV	icorr μA cm^{-2}	$-\beta c$ mV dec^{-1}	βa mV dec^{-1}
0	-283	0.164	138	349
100	-342	0.091	138	354
200	-467	0.087	139	360
400	-549	0.085	137	363
1000	-553	0.079	139	375

Fig.1 shows the polarization curves for carbon steel in saturated $Ca(OH)_2$ solution without and with different concentrations of HASI. The relevant electrochemical parameters such as the corrosion potential (E_{corr}), the corrosion current density (i_{corr}), the cathodic (β_c) and anodic Tafel slops (β_a) obtained through fitting the polarization data by the Tafel extrapolation method were collected in Table 1.

As shown in Fig.1, the polarization curves have the similar behavior for carbon steel samples in saturated $Ca(OH)_2$ solutions with and without the inhibitor during the entire polarization process, suggesting that the addition of the inhibitor did not change the anodic and cathodic reaction mechanism of carbon steel. These curves clearly show that at the initial stage of the anodic polarization, an obvious Tafel zone can be observed in the vicinity of OCP for all cases. This indicates that in this region, anodic active dissolution of iron occurred with the increasing of polarization potentials [15]. However, due to there were plenty of OH^- ions in the alkaline solution, they would react with the Fe^{2+} ions dissolved, leading to the formation of a precipitated protective film on carbon steel surface that hinders the further dissolution of iron. As the anodic polarization potential moved to more positive values, a further oxidation of Fe^{2+} to Fe^{3+} occurred and consequently an oxide film presumably with the composition of Fe_3O_4 or/ and Fe_2O_3 was formed, as a result, the electrode got into the passive state. This can be further confirmed by the fact that a plateau of passive current density occurred in the anodic polarization branches. When the polarization potential was about 700 mV, the pitting corrosion was accompanied by a sharp increase in the current density for all cases, and all the pitting potentials were higher than the potential of oxygen evolution. This phenomenon can be attributed to the depletion of local OH^- on the electrode surface due to the oxygen evolution.

However, it is worth noting that after the addition of HASI, there are two distinctive changes in comparison with the polarization behavior of electrode in blank solution: (i) both the corrosion current densities and the passive current densities decreased with the increasing concentration of HASI (see Table 1), implying that the reaction activities of carbon steel were reduced by the inhibitor. This can be ascribed to that the inhibitor molecule has multiple adsorption centers which enable it to adsorb on the electrode surface and suppress the anodic dissolution of iron. (ii) The corrosion potential shifted to the more negative values and the passive region of carbon steel became wider. These results indicate that the inhibitor can simultaneously retard both the anodic dissolution of iron and the cathodic oxygen reduction, but the inhibition effect to the cathodic reaction is much stronger than that to the anodic dissolution of iron, causing a definite negative shift of the corrosion potential (Table 1). There are two

possible reasons for the above experimental phenomena. The one is that the ferric and ferrous ions generated on the electrode surface interacted with the inhibitor molecules and led these ions to be constraint at a potential lower than the potential of oxides formation [2]. The other one is that by adsorption on carbon steel surface, the inhibitor blocked the adsorption and reduction of oxygen, and then inhibited the cathodic corrosion process [16].
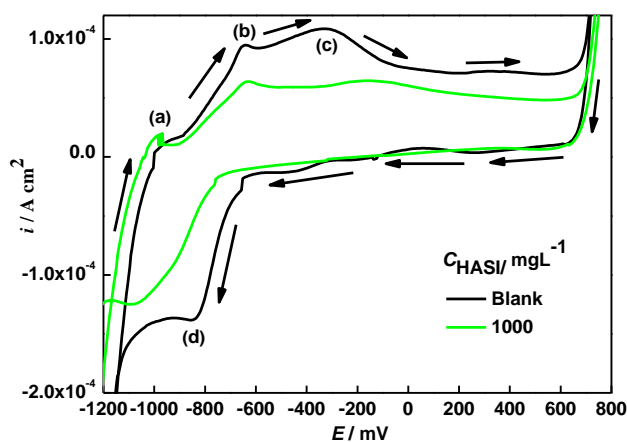

Figure 2. Cyclic voltammetry curves for carbon steel samples in saturated $Ca(OH)_2$ solutions without and with 1000 mgL^{-1} HASI

In order to further understand the effect of the inhibitor on the oxidation process of carbon steel sample, cyclic voltammetry curves were recorded in saturated $Ca(OH)_2$ solutions without and with 1000 mg L^{-1} HASI, as shown in Fig. 2.

It is evident that there are four peaks visible in the cyclic voltammetry curve of carbon steel electrodes in the blank solution. Three oxidation peaks occurred at the potential of −1100 mV (a), −700 mV (b) and −400 mV (c), respectively. The reduction peak (d) appeared at −800 mV. The peak (a) can be ascribed to the reaction of Fe→ Fe^{2+}, at which the product of iron dissolution, Fe^{2+} ions react with OH$^-$ to forme $Fe(OH)_2$ [2,17,18]. Due to the lower solubility of $Fe(OH)_2$, it could precipitate on the carbon steel surface and inhibit the carbon steel corrosion in some extent. The peak (b) can be assigned to the further oxidization of the ferrous ions into ferric species, where $Fe(OH)_2$ probably transform into the iron oxides and/or hydroxides following the reaction $Fe(OH)_2 \rightarrow Fe_3O_4/\alpha\text{-}Fe_2O_3$ (α-FeOOH) [2,17,18]. These compounds will cover the surface of carbon steel and hinder further the anodic dissolution of iron. Peak (c) can be attributed to the oxidation reaction as $Fe_3O_4 \rightarrow \gamma\text{-}Fe_2O_3$ (γ-FeOOH) [2,17,18]. Owing to that the γ-Fe_2O_3 (γ-FeOOH) has a more compact structure than that of the α-Fe_2O_3 (α-FeOOH), it could protect the carbon steel from the corrosion, hence resulting in the decrease in anodic current density after peak (c) and the carbon steel got into the passive state. During the backward scan, the corresponding reduction peak (d) of ferric species to ferrous ones can be clearly observed.

After the addition of an inhibitor, however, it is apparent that during the forward scan process, the corresponding oxidation peaks became smaller compared with those in the blank solution, while the anodic current density decreased. This phenomenon became more significant when the scan potentials were above –700 mV. These results indicate that in the inhibited solution, the inhibitor can largely reduce the formation of iron oxides and hydroxides due to the covering of inhibitor molecules on the carbon steel surface, and the adsorbed inhibitor molecules not only effectively suppressed the anodic active dissolution of iron, but also enhanced the stability of ferrous species to be further oxidized into ferric ones. Moreover, it can be seen that in the backward scan, the reduction peak (d) of ferric species transformation into ferrous ones disappeared, indicating that the reduction reactions of ferric oxides are largely retarded due to the interactions between adsorbed inhibitor molecules and oxides. According to the studies by Calvo et al. [19-21], in alkaline solution, the reduction of oxygen only occurs in the potential range where the iron oxides is reduced, and when there are both ferric and ferrous cations in the passive film, the reversible reaction between Fe^{2+} and Fe^{3+} has a strong catalytic effect for the O_2 reduction. So, when HASI was added to the solution, it could preferably adsorb on the oxides surface and block the access of oxygen dissolved in solution with the iron oxides, subesequently supressing the cathodic reduction of oxygen. This is why the inhibitor acted as a cathodic type inhibitor.

3.2 Raman spectra analysis

For determining the effect of inhibitor on the compositions of oxide film formed in alkaline solution, Fig. 3 depicts the Raman spectra for carbon steel samples after 3 days immersion in test solutions without and with 1000 mg L^{-1} HASI. For the sample in the blank solution, a strong peak at 508 cm^{-1} with a smaller band at 368 cm^{-1} can be observed, which can be assigned to Fe_2O_3 and ferrihydrite, indicating the compositions of the oxide film formed in the blank solution are mainly composed of ferric oxides and/or hydroxides [22,23].
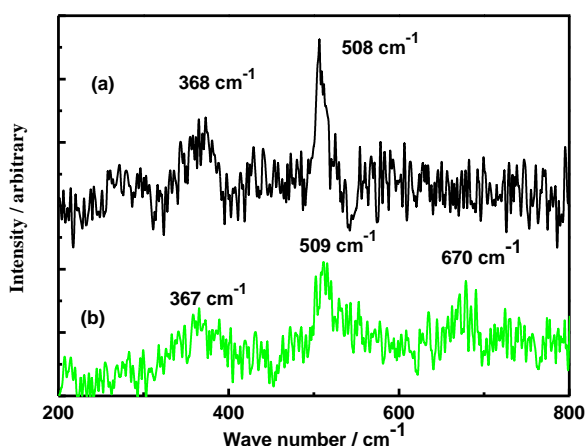

Figure 3. Raman spectra for carbon steel specimens after 3 days immersion in the test solution (a) blank; (b) with 1000 mg L^{-1} HASI

However, in the presence of HASI, not only the peaks of ferric substances occurred at 367 cm^{-1} and 509 cm^{-1}, but a peak at 670 cm^{-1} assigned to the Fe_3O_4 also appeared in the spectrum [22, 23], suggesting that by the adsorption on carbon steel surface, the inhibitor effectively improve the stability of Fe_3O_4 to be further oxidized into ferric species and enable it to exist, even under the atmosphere O_2 conditions. There results are totally in good agreement with those obtained by the cyclic voltammetry.

3.3 Electrochemical impedance spectroscopy (EIS)

Fig. 4 displays the Nyquist (a) and Bode (b) plots for carbon steel in test solutions without and with various concentrations of inhibitor. As would be expected, after the addition of inhibitor, the diameters of the capacitive semicircles gradually increased with increasing concentrations of HASI, indicating an improvement of protective performance of surface film formed on electrode surface due to the increasing amount of inhibitor molecules adsorbed on electrode surface, and the activity of carbon steel was effectively reduced [6,24,25]. Moreover, in the blank solution, only one phase
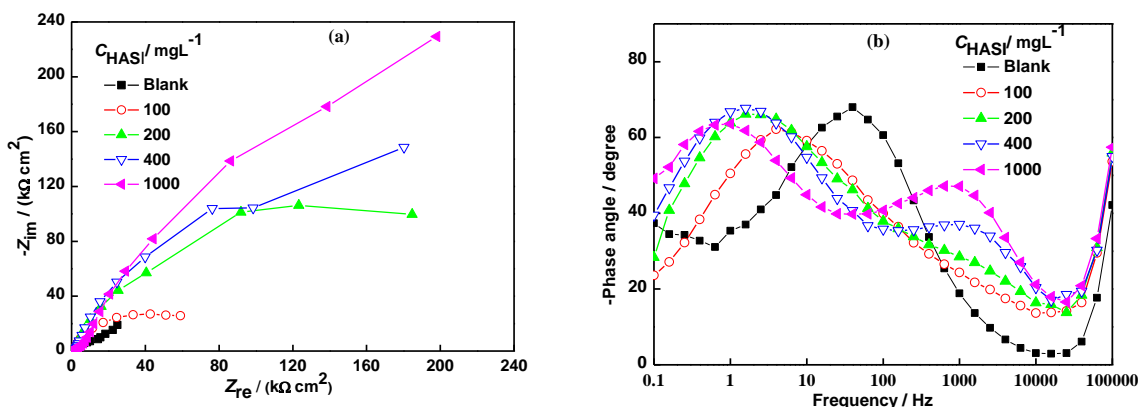

Figure 4. Nyquist (a) and Bode (b) plots for carbon steel in saturated $Ca(OH)_2$ solutions with different concentrations of HASI

angle maximum appeared in the Bode diagram, suggesting that the impedance of carbon steel in blank solution has one time constant, which reflects the electrochemical corrosion of carbon steel in test solution is dominantly controlled by the charge transfer process. However, after the addition of HASI, it is apparent that there are two phase angle maximums in the Bode plots, which are corresponding to the two capacitive loops in the Nyquist plots, indicating that the impedance of carbon steel in the inhibited solution is composed of two time constants. The first time constant at high frequencies is ascribed to the protective film formed on electrode surface, which consists of the adsorbed inhibitor molecules, iron oxides and hydroxides [14, 26], while the second time constant at low frequencies is related to the electron charge transfer process, corresponding to the time constant in the blank solution. Therefore, the impedance results can be interpreted by the equivalent circuit shown in Fig. 5. Fig. 5a

was used to fit the impedance behavior of carbon steel in the blank solution and Fig. 4b was used for the inhibited solution, respectively.

In the Fig. 5, R_s represents the solution resistance, R_f is the film resistance, R_{ct} represents the charge transfer resistance of the electric double layer. Considering the roughness and in-homogeneities of solid electrode surface, here, the constant phase elements CPE_1 and CPE_2 are used to replace the film capacitance and the double layer capacitance, respectively, and its value can be assessed by the following equation [27,28]:

$$Z_{CPE}(\omega) = Y_0^{-1} (j\omega)^{-n} \qquad (1)$$

where, Y_0 is the CPE constant, ω is the angular frequency (in rad/s), $j^2 = -1$, is the imaginary number and n is the CPE exponent. Depending on n, CPE can represent resistance [$Z_{CPE} = R$, $n = 0$], capacitance [$Z_{CPE} = C$, $n = 1$], inductance [$Z_{CPE} = L$, $n = -1$] or Warburg impedance for ($n = 0.5$) [23]. The obtained impedance parameters are listed in Table 2.
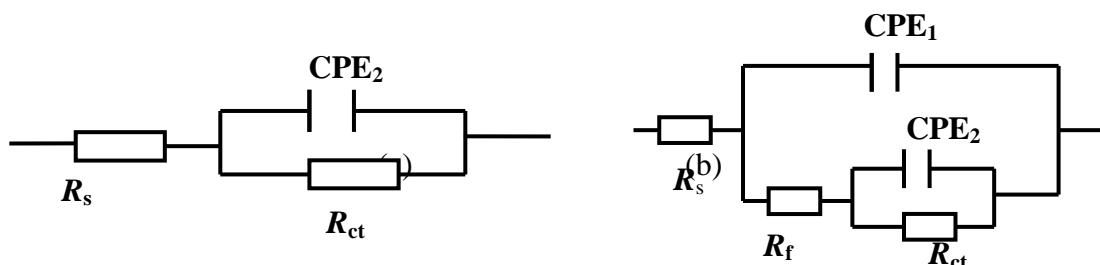

Figure 5. Equivalent circuits for impedance fitting (a) for the uninhibited solution; (b) for the inhibited solution

Table 2. The fitting results from the EIS data for carbon steel in saturated $Ca(OH)_2$ solutions with different concentrations of HASI

Conc.	Rs	CPE1		Rf	CPE2		Rct
		Y0-CPE1	n1		Y0-CPE2	n2	
mg L–1	Ω cm2	μΩ−1 Sn cm−2		kΩ cm2	μΩ−1 Sn cm−2		kΩ cm2
Blank				296	30.1	0.75	1.32
100	196	13.4	0.80	339	23.9	0.32	83.6
200	168	9.12	0.78	804	8.25	0.88	119
400	144	8.38	0.77	1976	8.01	0.93	126
1000	140	8.13	0.73	3880	6.92	0.89	256

From Table 2, it can be seen that the values of R_f and R_{ct} increased, whereas the values of Y_0 that represents CPE_1 and CPE_2 decreased with increasing concentration of HASI, which suggests that the amount of HASI molecules adsorbed on the electrode surface gradually increase and the inhibition

characteristics of the protective film formed on carbon steel surface is gradually improved. The increasing in values of R_f indicates that the development of a compact protective film on electrode surface by the adsorption of inhibitor, thereby enhancing the corrosion resistance of carbon steel [29]. The decrease in the capacitance values ($Y_{0\text{-CPE1}}$) may be related to the displacement of water and corrosion products on carbon steel surface by the adsorbed inhibitor molecules [6,29]. The reduction in values of $Y_{0\text{-CPE2}}$ can be ascribed to a decrease in the dielectric constant or an increase in the double electric layer thickness due to the inhibitor adsorption on electrode surface [27,28]. The increasing of R_{ct} reveals that the charge transfer reactions occurring in the protective film are strongly restricted after the addition of inhibitor [27,28]. These results reflect that the surface structure of electrode is modified and its protection property is significantly enhanced.

3.4 Mott–Schottky measurements

Previous researches have shown that passive films formed on most metals and alloys exhibit semiconductor behavior and Mott–Schottky measurements can be used to characterize the electronic properties of passive film and to identify the effect of inhibitor on the characteristic of surface film [30]. According to Mott–Schottky theory, the relationship between the space charge capacitance and the potential can be expressed as the following equation for an n-type semiconductor [31]:

$$\frac{1}{C^2} = \frac{2}{\varepsilon\varepsilon_o qN_d}(E - E_{fb} - \frac{kT}{q}) \tag{2}$$

where, N_d is the donor density, ε is the dielectric constant (here the value is 12 for the film formed on carbon steel [30]), ε_0 is the vacuum permittivity, q is the electron charge (1.602×10^{-19} C), k is the Boltzman constant, T is the absolute temperature, and E_{fb} is the flat band potential.
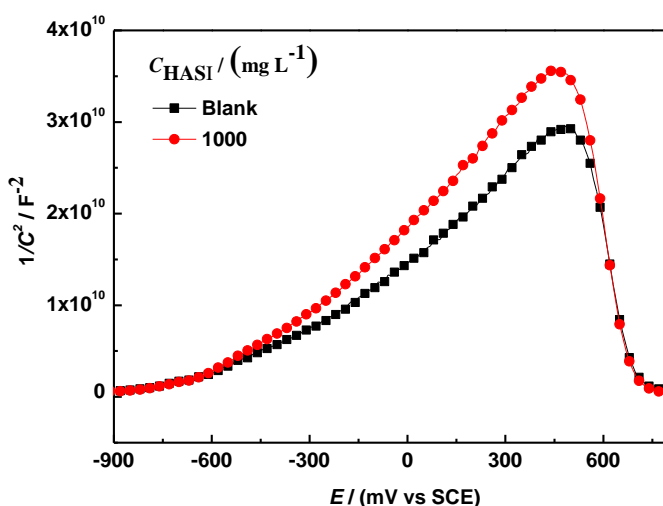

Figure 6. Mott–Schottky curves for carbon steel samples in saturated Ca(OH)$_2$ solutions without and with 1000 mgL^{-1} HASI

Table 3. The calculated results from the Mott–Schottky curves for carbon steel in saturated Ca(OH)$_2$ solutions without and with 1000 mg L^{-1} HASI

Conc. (mg L-1)	Efb (V)	Nd (cm-3)
0	-0.622	4.67 × 1020
1000	-0.609	3.92 × 1020

The values of N_d and E_{fb} can be estimated from the slope and intercept of the linear part of $1/C^2$ versus E curves, respectively.

Fig. 6 displays the Mott-Schottky plots for carbon steel in test solutions without and with 1000 mg L^{-1} HASI. The values of N_d and E_{fb} were calculated by fitting the curves in the potential range of -600 to -400 mV and listed in Table 3.

Fig. 6 clear shows that the reciprocal of C^2 increased with increasing potential in all cases, suggesting that the film formed on carbon steel surface exhibits an n-type semiconductor behavior. Also, the slop of Mott-Schottky curve in the inhibited solution was larger than that in the uninhibited solution, which indicates that the addition of inhibitor results in a decrease in the donor concentration inside the protective film formed with the inhibitor (see Table 3) and accordingly an increase in the protective performance of film. It has been confirmed that the oxide film formed on the steel surface has a spinel structure with multiple defects on the octahedral and tetrahedral sites, which will favor the penetration of the cations or anions across the oxide film and leads to the consumption of metals [32,33]. Thus, when such an oxide film is formed on the steel surface, the corrosion rate of steel could be reduced, but the corrosion is not stopped. This is because of abundant oxygen vacancies and insufficiently coordinated cations existing at the oxides/solution interface. This situation will facilitate the adsorption of the aggressive ions on them. However, in the presence of HASI, the inhibitor can influence the properties of oxide film formed on carbon steel surface by following two ways: (i) by an effective adsorption on carbon steel surface covered by oxides and/or participating in the formation process of oxide film, and hence to improve the structure of the double layer and decrease the active sites necessary for the coupled dissolution reaction of iron, (ii) by occupying the positions of oxygen vacancies and consequently to reduce the effective oxygen vacancy concentration and enhance the energy barrier for the electrochemical reaction, subsequently retarding the oxygen reduction reaction on the oxides surface. Therefore, after the addition of inhibitor, the corrosion resistance of oxide film was enhanced. These are in good agreement with the results of other electrochemical measurements.

3.5 Computational modeling

In order to clarify the influence of inhibitor on the properties of oxide film formed on carbon steel surface, computational modeling was performed by Material Studio software and the optimized results are shown in Fig.7.

From Fig. 7b, it can be seen that when the oxides surface contacted with the solution, the crystal structure of Fe$_3$O$_4$ covered on carbon steel surface became more disorder compared with that

before immersion in the blank solution (Fig. 7a) due to the interactions between the oxides and water molecules, which could lead to the further dissolution of oxides. Also, Fig. 7b clear shows that the cations on top of the oxide surface are apt to separate from the oxide matrix and diffuse into the bulk solution.
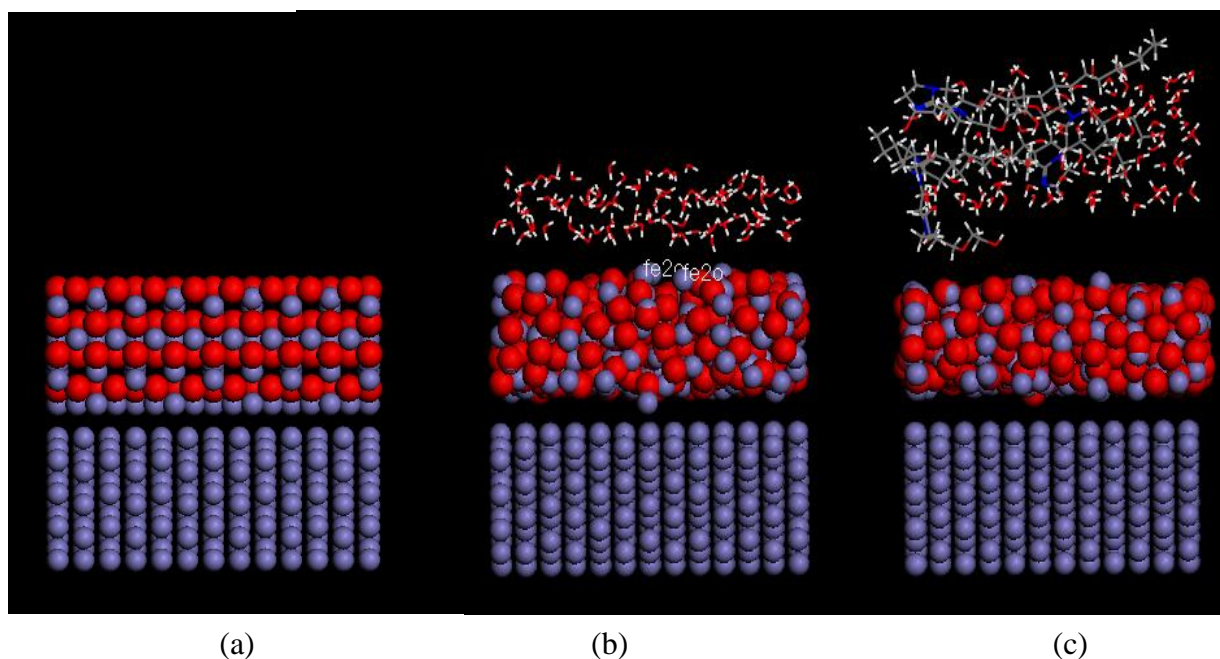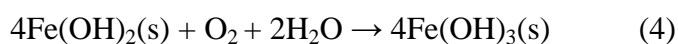

| (a) | (b) | (c) |

Figure 7. Computational simulation results for the influence of inhibitor on oxide film formed on carbon steel surface (a) oxide film before immersion in the solution; (b) oxide film in the blank solution; (c)oxide film in the solution with HASI

These results indicate that Fe_3O_4 is not stable in the blank solution, which tends to transform into ferric compounds by the following reactions:

$$3Fe_3O_4\,(s) + 2OH^- \rightarrow 4Fe_2O_3\,(s) + Fe(OH)_2(s) \qquad (3)$$

$$4Fe(OH)_2(s) + O_2 + 2H_2O \rightarrow 4Fe(OH)_3(s) \qquad (4)$$

So, in this case, the surface film formed is loose, porous and has the poor protective property. In the presence of inhibitor (Fig. 7c), however, it can be seen that the crystal structure of Fe_3O_4 is more complete and the oxide film is thinner than that in the blank solution, indicating that in the presence of inhibitor, the surface film formed is more compact and has fewer defects. These results suggest that the further oxidation of Fe_3O_4 is suppressed by the adsorption of inhibitor and the protective performance of oxide film is significantly improved.

4. MECHANISM ANALYSIS

Such an influence of the inhibitor on properties of surface film formed on carbon steel samples can be elucidate with the aid of point defect model (PDM) proposed by Macdonald (Fig.8) [37,38].
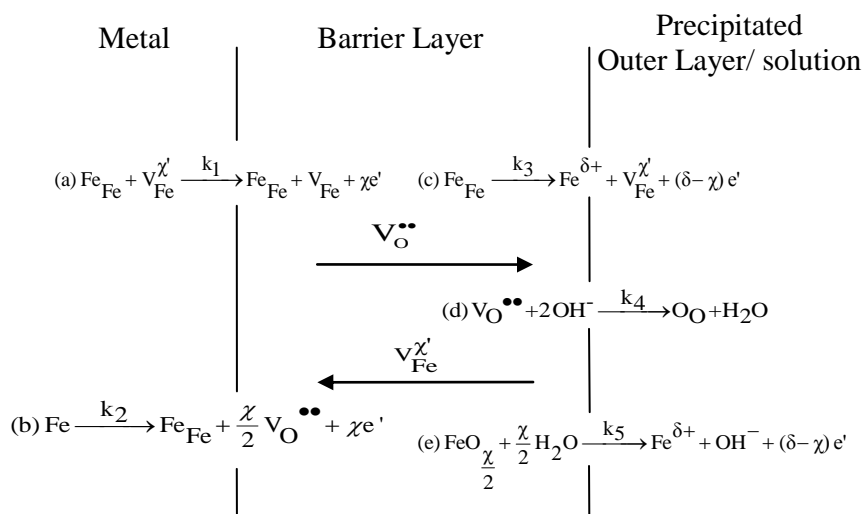

Figure 8. Schematic description of the point defect model proposed by Macdonald

Generally, in alkaline solution, the oxide film formed on the carbon steel surface has a bi-layer structure. The inner is a barrier layer composed mainly by Fe_3O_4 and has an n-type semiconductor behavior, while the outer is a porous layer consisted by hydroxides and oxyhydroxides. According to the PDM model, defects reactions (a) and (e) occur at metal/inner layer interface, namely, iron looses electrons to form ferrous and ferric ions, which are accompanied by the generation of oxygen vacancies. It should be noticed that the above two reactions occur in the solid phase and do not directly result in the dissolution of solid phase. At the outer layer/solution interface, cations can transfer into the liquid phase by means of reactions (c) and (d), leading to the dissolution of surface oxide film and the corrosion of substrate metal. Thus, the structure of oxide film plays an important role in the metal corrosion process, i.e. the defect density of the inner layer determines the speed of mass transfer, while the characteristic of the outer layer decides the process of electrochemical reaction. When the inhibitor is added into the solution, it can influence the corrosion characteristics of both inner and outer layers. First, the inhibitor participates in the formation process of surface film by adsorption on steel surface, which results in a decrease in the defect density of surface film and enhances the energy barrier for the mass and charge transference, consequently leading to a remarkable decrease in the reaction activity of surface film. Second, the outer layer structure can be modified by the inhibitor through the following ways: (i) by interactions with the cations produced by the reactions (c) and (e), hindering cations to enter into the solution and hence suppressing the dissolution of surface film. (ii) by adsorption on the oxides surface to form a blocking layer, inhibiting reactions (c), (d) and (e). Therefore, after addition of the inhibitor, the protection property of the surface film is greatly improved.

5. CONCLUSIONS

(1) HASI can effectively inhibit the carbon steel corrosion in saturated $Ca(OH)_2$ solution by suppressing dominantly the cathodic oxygen reduction.

(2) The inhibition activity of the inhibitor can be ascribed to the multiple functional groups existing in the molecular structure, which facilitates its adsorption on the oxides surface, leading to the formation of a protective film.

(3) The adsorption of HASI can result in two changes in the oxide film formed on carbon steel surface. (i) The defect density in oxide film is decreased and the stability of inner layer Fe_3O_4 is enhanced. (ii) The outer layer is modified by the adsorbed inhibitor molecules, which blocks the transport route for the reactions of mass and charge transfer, hence inhibiting both the anodic active dissolution of iron and the cathodic oxygen reduction.

References

1. T. A. Söylev, M. G. Richardson, *Constr. Buil. Mater.*, 22 (2008) 609.
2. S. Martinez, L. Valek, I. S. Oslakovic, *J. Electrochem. Soc.*, 154 (2007) C671.
3. L. Fedrizzi, F. Azzolini, P. L. Bonora, *Cement Concrete Res.*, 35 (2005) 551.
4. V. T. Ngala, C. L. Page, M. M. Page, *Corros. Sci.*, 45 (2003) 1523.
5. M. Ormellese, M. Berra, F. Bolzoni, T. Pastore, *Cement Concrete Res.* , 36 (2006) 536.
6. H.E. Jamil, A. Shriri, R. Boulif, C. Bastos, M.F. Montemor, M.G.S. Ferreira, *Electrochim. Acta*, 49 (2004) 2753.
7. U. Angst, B. Elsener, C.K. Larsen, Ø. Vennesland, *Cement Concrete Res.* 39 (2009)1122.
8. S.M.A. El Haleem, S.A. El Wanees, E.E.A. El Aal, A. Diab, *Corros. Sci.* 52 (2010)292.
9. B. Elsener, E. Zurich, in: M. Raupach, B. Elsener, R. Polder, J. Mietz (Eds.), Corrosion of Reinforcement in Concrete: Mechanisms, Monitoring, Inhibitors and Rehabilitation Techniques, 1st ed., Woodhead Publishing Limited, Cambridge, England, 2007, p. 170.
10. L.B. Mechmeche, L. Dhouibi, M. Ben Ouezdou, E. Triki, F. Zucchi, *Cement Concrete Compos.* 30 (2008) 167.
11. N. Etteyeb, L. Dhouibi, H. Takenouti, M.C. Alonso, E. Triki, Appl. *Electrochim. Acta* 52 (2007) 7506.
12. J. M. Wang, Y. Lu, J. Zhang, C. Cao, *Corros.Sci.*, 40 (1998) 1161.
13. J. J. Fu, S. N. Li, L. H. Cao, Y. Wang, L. H. Yan, L. D. Lu. J, *Mater. Sci.*, 45 (2010) 979.
14. L. J. Feng, H. Y. Yang, F. H. Wang, *Electrochim. Acta*, 58 (2011) 427.
15. E. M. Sherif, R. M. Erasmus, J. D. Comins, *J. Appl. Electrochem.*, 39 (2009) 83.
16. J. M. Gaidis. *Cement Concrete Compos.*, 26 (2004) 181.
17. S. Joiret, M. Keddam, X. R. Novoa, M. C. Perez, C. Rangel, H. Takenouti, *Cement Concrete Compos.*, 24 (2002) 7.
18. J. Flis, I. F. Kabulska, T. Zakroczymski, *Electrochim. Acta*, 54 (2009) 1810.
19. E. J. Calvo, D. J. Schiffrin, *J. Electroanal. Chem.*, 243 (1988) 171.
20. E. R. Vago, E. J. Calvo, *J.Electroanal. Chem.*, 339 (1992) 41.

21. E. R. Vago, E. J. Calvo, M. Stratmann, *Electrochim. Acta*, 39 (1994) 1655.
22. W. C. Baek, T. Kang, H. J. Sohn, Y. T. Kho, *Electrochim. Acta*, 46 (2001) 2321.
23. C. Gabrielli, S. Joiret, M. Keddam, *J. Electrochem. Soc.*, 153 (2006) B 68.
24. M.B. Valcarce, M. Vázquez, *Electrochim. Acta*, 53 (2008) 5007.
25. E. Machnikova, K.H. Whitmire, N. Hackerman, *Electrochim. Acta* 53 (2008) 6024.
26. H. Y. Du, X. M. Lu, Y. S. Wu, W. M. Wu, *Acta Metall. Sin.*, 42 (2006) 533.
27. X. Wang, H. Yang, F. Wang, *Corros. Sci.* 52 (2010) 1268.
28. M. Salasi, T. Shahourabi, E. Roayaei, M. Aliofkhazraei, *Mater. Chem. Phys.* 104(2007) 183.
29. L. Valek, S. Martinez, D. Mikulic, I. Brnardi´ c, *Corros. Sci.* 50 (2008) 2705.
30. H. Tsuchiya, S. Fujimoto, O. Chihara, T. Shibata, *Electrochimi. Acta*, 47 (2002) 4357.
31. V. Horvat-Radosevic, K. Kvastek, *Electrochimi. Acta,*. 42 (1997) 140.
32. E. Sikora, D. D. Macdonald, *J. Electrochem. Soc.*, 147 (2000) 4087.
33. M. Salasi, T. Shahourabi, E. Roayaei, M. Aliofkhazraei, *Mater. Chem. Phys.* 104 (2007) 183.
34. D.D.Macdonald, *J. Electrochem. Soc.*,139 (1992) 3434.
35. J. Liu, D. D. Macdonald, *J.Electrochem. Soc*., 148 (2001) B425.